HHS Public Access

Author manuscript

Magn Reson Med. Author manuscript; available in PMC 2022 January 01.

Published in final edited form as:

Magn Reson Med. 2022 January ; 87(1): 409–416. doi:10.1002/mrm.28973.

Contribution of blood to nuclear Overhauser effect at −1.6 ppm

Jing Cui[1,2], **Yu Zhao**[1,2], **Feng Wang**[1,2], **Daniel F. Gochberg**[1,2,3], **Zhongliang Zu**[1,2]

[1]Vanderbilt University Institute of Imaging Science, Nashville, US

[2]Department of Radiology and Radiological Sciences, Vanderbilt University Medical Center, Nashville, US

[3]Deparment of Physics and Astronomy, Vanderbilt University, Nashville, US

Abstract

Purpose: A relayed nuclear Overhauser enhancement (rNOE) saturation transfer effect at around −1.6 ppm from water, termed NOE(−1.6), was previously reported in rat and human brain, and some publications suggest that it may be related to blood. Here, we studied whether the NOE(−1.6) arises from blood through *in vivo* and *ex vivo* experiments.

Methods: To evaluate the contribution from *in vivo* blood to NOE(−1.6), intravascular signals in rat brain were suppressed by two approaches: (1) signal acquisition with a diffusion-weighting of b = 400s/mm^2; (2) intravascular injection of 5 mg/kg monocrystalline iron oxide nanoparticle (MION). *Ex vivo* blood sample was also prepared. The signals were acquired using a chemical exchange saturation transfer (CEST) pulse sequence. Multiple-pool Lorentizan fitting of CEST Z-spectra was performed to quantify the NOE(−1.6) signal.

Results: There are no significant variations in the fitted *in vivo* NOE(−1.6) signals when measured with or without diffusion-weighting, but significant signal decease does occur after injection of MION. The NOE(−1.6) signal from *ex vivo* blood is weaker than that from *in vivo* tissues.

Conclusion: Considering the relatively small volume of blood in brain, the *in vivo* experiments with diffusion weighting and the *ex vivo* experiments both suggest that the NOE(−1.6) is not mainly from blood. The mechanism for the *in vivo* experiments with MION are less clear. MION not only suppresses MR signals from intravascular space, but changes the susceptibility in the perivascular space. This result suggests that although the NOE(−1.6) is not mainly from blood, it may be vasculature dependent.

Keywords

chemical exchange saturation transfer (CEST); nuclear Overhauser enhencement (NOE); NOE(−1.6)

Correspondence to: Zhongliang Zu, Ph.D., Vanderbilt University Institute of Imaging Science, 1161 21st Ave. S, Medical Center North, AAA-3112, Nashville, TN 37232-2310, zhongliang.zu@vumc.org.

INTRODUCTION

Chemical exchange saturation transfer (CEST) has emerged as an important contrast mechanism for detecting endogenous and exogenous molecules with protons that chemically exchange or have (a possibly multi-step interaction) cross-relaxation with water protons. Such protons can be selectively saturated by a long (e.g. a couple seconds) off-resonance RF irradiation pulse and the saturation is subsequently transferred to bulk water, causing an accumulative attenuation in water signal. By measuring the change in water signal, the solute protons can be indirectly detected with relatively high sensitivity.

In CEST imaging, a Z-spectrum, the plot of water signal as a function of RF irradiation frequency, is usually created so that all exchanging and 'coupling' effects can be identified (1). In previous studies, multiple effects have been observed in biological tissues, including amide proton transfer (APT) at ~3.5 ppm (2-4), amine-water exchange effect at ~2 ppm (5-12), and relayed nuclear Overhauser enhancement (rNOE) saturation transfer effects at ~−1.6 ppm (NOE(−1.6)) (13-21) and ~−3.5 ppm (NOE(−3.5)) (22-31). However, although the origin of the amide, amine, and NOE(−3.5) CEST effects have been well studied, the origin of the NOE(−1.6) is still controversial. Understanding its biophysical origins in tissues may lead to novel and exploitable MR contrast mechanisms.

In general, NOE originates from through-space dipole-dipole interactions (32-34). Previously, we have tentatively assigned the NOE(−1.6) to be from dipolar interactions between phospholipid choline head group protons and water protons (14,15,19). Recently, we have reported that the NOE(−1.6) signal from rat brain changes significantly with intake of different gases (i.e. air, O_2, and N_2O) (16), suggesting that the NOE(−1.6) signal may be related to cerebrovascular reactivity. Two other publications also observed the NOE(−1.6) signal in blood (17,18). In this paper, we evaluated whether the NOE(−1.6) signal arises from blood by using two *in vivo* blood suppression approaches and an *ex vivo* blood sample.

We suppressed the blood signal via diffusion gradients and relaxation agent compartmentation. In biological tissues, the structure of microvasculature is random and the blood flow in large vessels is laminar. Based on the intravoxel incoherent motion (IVIM) model (35), when moderate diffusion weighting from diffusion gradients is applied during the signal acquisition, intravascular signals from an imaging voxel can be effectively suppressed, but the extravascular signals do not reduce greatly (36-39). Here, we acquired CEST signals with/without moderate diffusion weighting during the signal acquisition to evaluate the contributions from *in vivo* blood to the NOE(−1.6). Our second approach used monocrystalline iron oxide nanoparticle (MION), which were usually used as a susceptibility agent with a long half-life, and which can reduce the water transverse relaxation time. Intravenous injection of MION can suppress signals from intravascular space and change the susceptibility in the perivascular space (40-42).

METHODS

Animal Preparation

All rats were immobilized and anesthetized with 2-3% isoflurane (ISO) and 97-98% oxygen (O_2) for both induction and maintenance during the experiments. Respiration rate was monitored to be in a range from 40 to 70 breaths per minute. Rectal temperature was maintained at 37°C using a warm-air feedback system (SA Instruments, Stony Brook, NY). Five rats were used for the CEST experiments with diffusion weighting during the signal acquisition. Five rats were used for the CEST experiments with injection of MION. All animal procedures were approved by the Animal Care and Usage Committee of Vanderbilt University.

Ex vivo blood Preparation

A rat was anesthetized with 2-3% isoflurane (ISO) and 97-98% oxygen (O_2). *Ex vivo* blood was then collected from the rat artery using a syringe containing lyophilized heparin, and moved quickly to a sealed tube immediately before the MRI scan.

MRI

All measurements were performed on a Varian DirectDrive™ horizontal 9.4 T magnet with a 38-mm Litz RF coil (Doty Scientific Inc. Columbia, SC). CEST measurements on animals were performed by applying a continuous wave (CW)-CEST sequence with a 5-s CW irradiation pulse followed by a single-shot spin-echo echo planar imaging (SE-EPI) acquisition. CEST measurements on the *ex vivo* blood sample were also performed by applying a CW-CEST sequence with 5-s CW irradiation pulse, but followed by a free induction decay (FID) acquisition so that they have high signal-to-noise ratio. The first points of each FID were used for data analysis. The delay time between two adjacent CW pulses is 2 s. The effective time of echo (TE) is 27 ms and 31 ms for the SE-EPI acquisition in the experiments with injection of MION and with diffusion weighting, respectively. Z-spectra were acquired with RF offsets at ±4000, ±3500, ±3000, ±2500, and from −2000 to 2000 Hz with a step of 50 Hz (−10 to 10 ppm on 9.4 T) and irradiation powers ($\boldsymbol{\omega}_1$) of 1 μT (43). Control images or signals (S_0) were obtained by setting the RF offset to 100 kHz (250 ppm on 9.4 T). Apparent water longitudinal relaxation rate (R_{1obs}) and semi-solid MT pool concentration (f_m) were obtained using a selective inversion recovery (SIR) method with inversion times of 4, 5, 6, 8, 10, 12, 15, 20, 50, 200, 500, 800, 1000, 2000, 4000, and 6000 ms (44). Before data acquisition, shimming was carefully performed so that the root mean square (RMS) deviation of B_0 was less than 5 Hz. All images were acquired with matrix size 64 × 64, field of view 30 × 30 mm^2, and one acquisition. For the diffusion weighted SE-EPI imaging, two unipolar gradients (Stejskal-Tanner) along all three axes with duration of 2 ms, separation of 12 ms, and amplitude of 200 mT/m (b = 400 s/mm^2) were applied on both sides of the 180° refocus pulse (45). Several previous publications (36-39) have indicated that moderate diffusion weighting can suppress the most of the intravascular signal. CEST and SIR measurements were applied with/without the diffusion gradients on animals. For the MION injection experiments, 5 mg/kg MION, which was shown to effectively suppress intravascular signals in several previous publications (40-42), were injected intravenously

to each rat. CEST and SIR measurements were applied before and after (within 1 h) the injection of MION.

Data analysis

Previously, it was reported that slow exchanging CEST effects as well as semi-solid MT and direct water saturation (DS) effects in a frequency range close to the water resonance can be modeled using Lorentzian functions (46). Here, we performed a multiple-pool Lorentzian fitting of Z-spectrum to isolate each peak. Eq. (1) provides the model function of the Lorentzian fit method.

$$\frac{S_{mea}(\Delta\omega)}{S_0} = 1 - \sum_{i=1}^{N} L_i(\Delta\omega) \quad (1)$$

Here, $L_i(\Delta\omega)=A_i/(1+(\Delta\omega-\Delta_i)^2/(0.5W_i)^2)$, which represents a Lorentzian line with central frequency offset from water (Δ_i), peak full width at half maximum (W_i), and peak amplitude (A_i). N is the number of fitted pools. The fitting has 6 pools including CEST(3.5), CEST(2), NOE(−1.6), and NOE(−3.5) representing the CEST/rNOE dips at 3.5 ppm, 2 ppm, −1.6 ppm, −3.5 ppm, as well as water at 0 ppm and semi-solid MT at −2.3 ppm. S_{mea} is the measured signal on the Z-spectrum, and Δω is the irradiation frequency offset from water. The fitting was performed to achieve the lowest RMS of residuals between the measured data and model. All fitting for *in vivo* experiments were performed voxel by voxel with images smoothed by a 3 × 3 median filter before fitting. Supporting Information Table S1 lists the starting points and boundaries of the fit.

The reference signal (S_{ref}) for quantifying a CEST or rNOE effect was obtained by the sum of all Lorentzians except the corresponding pool. Magnetization transfer ratio (MTR), which is the difference of S_{ref} and the measured signal (S_{mea}), has been traditionally used to quantify the CEST or rNOE effect. However, MTR values depend not only on CEST or rNOE effects, but also on other tissue parameters including direct water saturation (DS), semi-solid MT, and water longitudinal relaxation rate ($R_{1w}=1/T_{1w}$) (47,48). Thus, the CEST or rNOE effects quantified by MTR across different biological tissues (e.g. blood and brain parenchyma) may not be compared fairly due to variations in R_{1w} and f_m. Here, we instead use a metric, termed exchange-dependent relaxation (AREX), to quantify CEST and rNOE effects with greater specificity to a single exchange mechanism (47). AREX spectra (Eq. (2)) were obtained by inversely subtracting S_{mea} from S_{ref} and correcting for R_{1obs}.

$$\mathrm{AREX}(\Delta\omega) = \left(\frac{S_0}{S_{mea}(\Delta\omega)} - \frac{S_0}{S_{ref}(\Delta\omega)}\right) R_{1obs}(1 + f_m) \quad (2)$$

Here, $1+f_m$ was added to make the inverse method more specific, as shown in the previous publication (47). The AREX values for CEST(3.5), NOE(−1.6) and NOE(−3.5) were obtained by choosing the maximum values in a frequency range from 3 ppm to 4 ppm, −1 ppm to −2 ppm, and −2.5 to 4.5 ppm, respectively, on the AREX spectrum. The AREX values for CEST(2) were not analyzed since there are multiple fast exchanging pools

close to 2 ppm, resulting in line shapes that are not single Lorentzians (49,50). Since we previously reported that the central frequency offset of the NOE(−1.6) shifts in different regions (14), the AREX map for NOE(−1.6) was created by the maximum values in a frequency range from −1 ppm to −2 ppm on the AREX spectrum for each voxel. The AREX spectrum and values from the whole brain and four different region of interests (ROIs) (CP, caudate putamen; CC, corpus callosum; SC, singular cortex; C, cortex) in the measured slice were analyzed. The ROIs were defined based on a T_{2w}-weighted anatomy image.

Statistics

Student's t-test were employed to evaluate the signal difference. It was considered to be statistically significant when $P < 0.05$. All data analysis and statistical analyses were performed using Matlab R2020a (Mathworks, Natick, MA, USA).

RESULTS

Fig. 1a and 1b show the average CEST Z-spectra and AREX spectra, respectively, from the whole brain of 5 rat brains acquired with diffusion weighting of b = 0 s/mm^2 (blue) and 400 s/mm^2 (red). The fitting residuals (Supporting Information Figure S1) are very low, indicating the success of the fitting. The average CEST Z-spectra and AREX spectra from other four ROIs acquired with/without the diffusion weighting are shown in Supporting Information Figure S2. Note that the CEST/rNOE dips at ~3.5 ppm, ~2 ppm, ~−1.6 ppm, and ~−3.5 ppm can be clearly observed on the Z-spectra. The AREX spectra shows the fitted peaks for these pools. Fig. 1c and 1d give the control images without/with the diffusion weighting, respectively, from a representative rat brain. Fig. 1e and 1f give the NOE(−1.6) images without/with the diffusion weighting, respectively, from a representative rat brain. Fig. 2 shows the statistical analysis of the fitted AREX values for CEST(3.5), NOE(−1.6), and NOE(−3.5) as well as the control signals from the whole brain without/with the diffusion weighting. The statistical analysis of the fitted AREX values from other four ROIs acquired with/without the diffusion weighting are shown in Supporting Information Figure S3. Note that although there are significant difference between the control signals acquired without/with diffusion weighting due to the loss of intravascular signals and diffusion effects, there are no statistical differences between the AREX values of the CEST and NOE data acquired without/with diffusion weighting, except that for the NOE(−1.6) from CP ($P = 0.022$). (The mean AREX value for NOE(−1.6) from CP only deceases by 16.4 % (from 11.4 %s^{-1} to 9.5 %s^{-1})).

Fig. 3 shows the CEST Z-spectrum and AREX spectrum from *ex vivo* blood. The fitting residuals (Supporting Information Figure S4) are very low, indicating the success of the fitting. Note that the CEST at ~3.5 ppm and ~2 ppm, rNOE dips at ~−1.6 ppm and ~−3.5 ppm can be clearly observed on the Z-spectra. Also note that although the fitted NOE(−3.5) from *ex vivo* blood (20.1 %s^{-1}) is higher than that from the *in vivo* tissue of the whole brain (16.3 %s^{-1} ± 1.6 %s^{-1}, b = 0 s/mm^2 in Fig. 2c), the fitted NOE(−1.6) from *ex vivo* blood (7.0 %s^{-1}) is lower than that from the *in vivo* tissue of the whole brain (10.1% s^{-1} ± 0.6 %s^{-1}, b = 0 s/mm^2 in Fig. 2b).

Fig. 4a and 4b show the average CEST Z-spectra and AREX spectra, respectively, from the whole brain of 5 rat brains acquired before and after the injection of MION. The fitting residuals (Supporting Information Figure S5) are very low, indicating the success of the fitting. The average CEST Z-spectra and AREX spectra from other four ROIs acquired before and after the injection of MION are shown in Supporting Information Figure S6. Note the disappearance of the rNOE dip at ~−1.6 ppm, but not dips at other frequency offsets, on the CEST Z-spectra acquired after the injection of MION. Fig. 4c and 4d give the control images before and after the injection of MION, respectively, from a representative rat brain. Fig. 4e and 4f give the NOE(−1.6) images before and after the injection of MION, respectively, from a representative rat brain. Fig. 5 shows the statistical analysis of the fitted AREX values for CEST(3.5), NOE(−1.6), and NOE(−3.5) as well as the control signals from the whole brain before and after the injection of MION. The statistical analysis of the fitted AREX values from other four ROIs acquired before and after the injection of MION are shown in Supporting Information Figure S7. The control signals from the whole brain decrease significantly by 16.5 % ± 3.6 %, suggesting the successful intravenous injection of MION. Note that the AREX values for NOE(−1.6) from the whole brain ($P < 0.001$), CP ($P < 0.001$), CC ($P = 0.001$), SC ($P = 0.002$), and C ($P = 0.002$) decrease significantly by 54.6 % (from 10.9 $\%s^{-1}$ to 4.9 $\%s^{-1}$), 53.4 % (from 11.9 $\%s^{-1}$ to 5.3 $\%s^{-1}$), 47.2 % (from 11.3 $\%s^{-1}$ to 6.0 $\%s^{-1}$), 67.8 % (from 14.1 $\%s^{-1}$ to 4.5 $\%s^{-1}$), and 56.0 % (from 11.3 $\%s^{-1}$ to 5.0 $\%s^{-1}$), respectively, after the injection of MION, suggesting the NOE(−1.6) is greatly influenced by MION. There are also significant changes of AREX values for CEST(3.5) from the whole brain ($P = 0.023$) and from SC ($P = 0.036$), and AREX values for NOE(−3.5) from SC ($P = 0.019$). However, the mean AREX value for CEST(3.5) from the whole brain and from SC, and AREX values for NOE(−3.5) from SC only decease by 14.6 % (from 5.7 $\%s^{-1}$ to 4.9 $\%s^{-1}$), 13.8 % (from 5.7 $\%s^{-1}$ to 5.0 $\%s^{-1}$), and −11.5 % (from 12.4 $\%s^{-1}$ to 13.8 $\%s^{-1}$), respectively, which are much smaller compared with the change of AREX value for NOE(−1.6).

DISCUSSION AND CONCLUSION

Previously, it was reported that b = 200-400 s/mm^2 is sufficient to suppress most the MR signals from large vessels and microvasculature where they are randomly orientated (39). Our *in vivo* experiments with diffusion weighting (b = 400 s/mm^2) thus indicates that blood, at least, is not a dominant contributor to NOE(−1.6) in live rat brain. The cerebral blood volume takes ~5% of rodent brain volume (51,52). If the NOE(−1.6) signal is only from blood, blood should have an AREX value of 202 $\%s^{-1}$ for the NOE(−1.6) (NOE(−1.6) of 10.1 $\%s^{-1}$ from the whole brain in Fig. 2b / 5%) which is much higher than the NOE(−1.6) value of 7.0 $\%s^{-1}$ from the *ex vivo* blood. This *ex vivo* experiment thus further suggests that the NOE(−1.6) signal should not be mainly from blood.

The mechanism for the significant change of NOE(−1.6) signal with injection of MION in the *in vivo* experiments is less clear. MION not only suppresses MR signals from intravascular space, but changes the susceptibility in the perivascular space. This *in vivo* experiment with MION suggests that although the NOE(−1.6) is not mainly from blood, it may arise from the perivascular space and may be relevant to vasculature. This experiment may also provide insight into the mechanism for the dependence of NOE(−1.6) on the gas

challenge studies in our previous publication (16) in which the vascular susceptibility always changes. Future studies on the mechanism and the exact location of the NOE(−1.6) signal are warranted.

The NOE(−1.6) is very close to water, and thus fitting errors due to the presence of DS effects may not be avoided even if the fitting residual is low. However, the DS effects in our experiments before and after the injection of MION are roughly close (Supporting Information Figure. S8). Thus their fitting errors may be similar, and our conclusion drawn from the different fitted NOE(−1.6) signals acquired before and after the injection of MION should be still valid. In addition, we found that the central frequency offset of the NOE(−1.6) shifts in different brain regions which is similar to our previous report (14) (Supporting Information Table S2 and S3).

Supplementary Material

Refer to Web version on PubMed Central for supplementary material.

REFERENCES

1. Zhou JY, van Zijl PCM. Chemical exchange saturation transfer imaging and spectroscopy. Prog Nucl Mag Res Sp 2006;48(2-3):109–136.
2. Zhou JY, Payen JF, Wilson DA, Traystman RJ, van Zijl PCM. Using the amide proton signals of intracellular proteins and peptides to detect pH effects in MRI. Nat Med 2003;9(8):1085–1090. [PubMed: 12872167]
3. Zhou JY, Lal B, Wilson DA, Laterra J, van Zijl PCM. Amide proton transfer (APT) contrast for imaging of brain tumors. Magn Reson Med 2003;50(6):1120–1126. [PubMed: 14648559]
4. Zhou JY, Tryggestad E, Wen ZB, Lal B, Zhou TT, Grossman R, Wang SL, Yan K, Fu DX, Ford E, Tyler B, Blakeley J, Laterra J, van Zijl PCM. Differentiation between glioma and radiation necrosis using molecular magnetic resonance imaging of endogenous proteins and peptides. Nat Med 2011;17(1):130–U308. [PubMed: 21170048]
5. Cai KJ, Singh A, Poptani H, Li WG, Yang SL, Lu Y, Hariharan H, Zhou XHJ, Reddy R. CEST signal at 2ppm (CEST@2ppm) from Z-spectral fitting correlates with creatine distribution in brain tumor. Nmr Biomed 2015;28(1):1–8. [PubMed: 25295758]
6. Cai KJ, Tain RW, Zhou XJ, Damen FC, Scotti AM, Hariharan H, Poptani H, Reddy R. Creatine CEST MRI for Differentiating Gliomas with Different Degrees of Aggressiveness. Mol Imaging Biol 2016;19(2):225–232.
7. Zhang XY, Xie JP, Wang F, Lin EC, Xu JZ, Gochberg DF, Gore JC, Zu ZL. Assignment of the molecular origins of CEST signals at 2ppm in rat brain. Magn Reson Med 2017;78(3):881–887. [PubMed: 28653349]
8. Chen L, Zeng HF, Xu X, Yadav NN, Cai SH, Puts NA, Barker PB, Li T, Weiss RG, van Zijl PCM, Xu JD. Investigation of the contribution of total creatine to the CEST Z-spectrum of brain using a knockout mouse model. Nmr Biomed 2017;30(12).
9. Chen L, Barker PB, Weiss RG, van Zijl PCM, Xu JD. Creatine and phosphocreatine mapping of mouse skeletal muscle by a polynomial and Lorentzian line-shape fitting CEST method. Magn Reson Med 2019;81(1):69–78. [PubMed: 30246265]
10. Singh A, Debnath A, Cai KJ, Bagga P, Haris M, Hariharan H, Reddy R. Evaluating the feasibility of creatine-weighted CEST MRI in human brain at 7 T using a Z-spectral fitting approach. NMR in biomedicine 2019;32(12).
11. Kogan F, Haris M, Singh A, Cai KJ, Debrosse C, Nanga RPR, Hariharan H, Reddy R. Method for High-Resolution Imaging of Creatine In Vivo Using Chemical Exchange Saturation Transfer. Magn Reson Med 2014;71(1):164–172. [PubMed: 23412909]

12. Haris M, Singh A, Cai KJ, Kogan F, McGarvey J, DeBrosse C, Zsido GA, Witschey WRT, Koomalsingh K, Pilla JJ, Chirinos JA, Ferrari VA, Gorman JH, Hariharan H, Gorman RC, Reddy R. A technique for in vivo mapping of myocardial creatine kinase metabolism. Nat Med 2014;20(2):209–214. [PubMed: 24412924]
13. Zhang XY, Wang F, Afzal A, Xu JZ, Gore JC, Gochberg DF, Zu ZL. A new NOE-mediated MT signal at around-1.6 ppm for detecting ischemic stroke in rat brain. Magn Reson Imaging 2016;34(8):1100–1106. [PubMed: 27211260]
14. Zhang XY, Wang F, Jin T, Xu JZ, Xie JP, Gochberg DF, Gore JC, Zu ZL. MR imaging of a novel NOE-mediated magnetization transfer with water in rat brain at 9.4T. Magn Reson Med 2017;78(2):588–597. [PubMed: 27604612]
15. Zu ZL. Ratiometric NOE(−1.6) contrast in brain tumors. Nmr Biomed 2018;31(12).
16. Zu ZL. Toward more reliable measurements of NOE effects in CEST spectra at around-1.6 ppm (NOE (−1.6)) in rat brain. Magnetic Resonance In Medicine 2019;81(1):208–219. [PubMed: 30058128]
17. Zaiss M, Schuppert M, Deshmane A, Herz K, Ehses P, Fullbier L, Lindig T, Bender B, Ernemann U, Scheffler K. Chemical exchange saturation transfer MRI contrast in the human brain at 9.4 T. Neuroimage 2018;179:144–155. [PubMed: 29894826]
18. Shah SM, Mougin OE, Carradus AJ, Geades N, Dury R, Morley W, Gowland PA. The z-spectrum from human blood at 7T. Neuroimage 2018;167:31–40. [PubMed: 29111410]
19. Zu ZL, Lin EC, Louie EA, Xu JZ, Li H, Xie JP, Lankford CL, Chekmenev EY, Swanson SD, Does MD, Gore JC, Gochberg DF. Relayed nuclear Overhauser enhancement sensitivity to membrane Cho phospholipids. Magnetic Resonance In Medicine 2020.
20. Heo HY, Jones CK, Hua J, Yadav N, Agarwal S, Zhou JY, van Zijl PCM, Pillai JJ. Whole-Brain Amide Proton Transfer (APT) and Nuclear Overhauser Enhancement (NOE) Imaging in Glioma Patients Using Low-Power Steady-State Pulsed Chemical Exchange Saturation Transfer (CEST) Imaging at 7T. J Magn Reson Imaging 2016;44(1):41–50. [PubMed: 26663561]
21. Zhou IY, Wang E, Cheung JS, Zhang X, Fulci G, Sun PZ. Quantitative chemical exchange saturation transfer (CEST) MRI of glioma using Image Downsampling Expedited Adaptive Least-squares (IDEAL) fitting. Scientific reports 2017;7(1):84. [PubMed: 28273886]
22. van Zijl PCM, Zhou J, Mori N, Payen JF, Wilson D, Mori S. Mechanism of magnetization transfer during on-resonance water saturation. A new approach to detect mobile proteins, peptides, and lipids. Magn Reson Med 2003;49(3):440–449. [PubMed: 12594746]
23. Jones CK, Huang A, Xu JD, Edden RAE, Schar M, Hua J, Oskolkov N, Zaca D, Zhou JY, McMahon MT, Pillai JJ, van Zijl PCM. Nuclear Overhauser enhancement (NOE) imaging in the human brain at 7 T. Neuroimage 2013;77:114–124. [PubMed: 23567889]
24. Zaiss M, Windschuh J, Paech D, Meissner JE, Burth S, Schmitt B, Kickingereder P, Wiestler B, Wick W, Bendszus M, Schlemmer HP, Ladd ME, Bachert P, Radbruch A. Relaxation-compensated CEST-MRI of the human brain at 7 T: Unbiased insight into NOE and amide signal changes in human glioblastoma. Neuroimage 2015;112:180–188. [PubMed: 25727379]
25. Khlebnikov V, Windschuh J, Siero JCW, Zaiss M, Luijten PR, Klomp DWJ, Hoogduin H. On the transmit field inhomogeneity correction of relaxation-compensated amide and NOE CEST effects at 7T. NMR in biomedicine 2017;30(5).
26. Khlebnikov V, Siero JCW, Wijnen J, Visser F, Luijten PR, Klomp DWJ, Hoogduin H. Is there any difference in Amide and NOE CEST effects between white and gray matter at 7 T? Journal Of Magnetic Resonance 2016;272:82–86. [PubMed: 27662404]
27. Desmond KL, Moosvi F, Stanisz GJ. Mapping of Amide, Amine, and Aliphatic Peaks in the CEST Spectra of Murine Xenografts at 7 T. Magn Reson Med 2014;71(5):1841–1853. [PubMed: 23801344]
28. Jones CK, Polders D, Hua J, Zhu H, Hoogduin HJ, Zhou JY, Luijten P, van Zijl PCM. In vivo three-dimensional whole-brain pulsed steady-state chemical exchange saturation transfer at 7 T. Magnetic Resonance in Medicine 2012;67(6):1579–1589. [PubMed: 22083645]
29. Lee DH, Heo HY, Zhang K, Zhang Y, Jiang SS, Zhao XN, Zhou JY. Quantitative assessment of the effects of water proton concentration and water T-1 changes on amide proton transfer (APT)

and nuclear overhauser enhancement (NOE) MRI: The origin of the APT imaging signal in brain tumor. Magnetic Resonance In Medicine 2017;77(2):855–863. [PubMed: 26841096]

30. Chung JJ, Choi W, Jin T, Lee JH, Kim SG. Chemical-exchange-sensitive MRI of amide, amine and NOE at 9.4T versus 15.2T. NMR in biomedicine 2017;30(9).
31. Jin T, Wang P, Zong XP, Kim SG. MR imaging of the amide-proton transfer effect and the pH-insensitive nuclear overhauser effect at 9.4 T. Magn Reson Med 2013;69(3):760–770. [PubMed: 22577042]
32. Anderson WA, Freeman R. Influence of a Second Radiofrequency Field on High-Resolution Nuclear Magnetic Resonance Spectra. J Chem Phys 1962;37(1):85-&.
33. Vogeli B. The nuclear Overhauser effect from a quantitative perspective. Progress in Nuclear Magnetic Resonance Spectroscopy 2014;78:1–46. [PubMed: 24534087]
34. Solomon I. Relaxation Processes in a System of 2 Spins. Physical Review 1955;99(2):559–565.
35. Lebihan D, Breton E, Lallemand D, Grenier P, Cabanis E, Lavaljeantet M. Mr Imaging Of Intravoxel Incoherent Motions - Application To Diffusion And Perfusion In Neurologic Disorders. Radiology 1986;161(2):401–407. [PubMed: 3763909]
36. Jin T, Wang P, Tasker M, Zhao FQ, Kim SG. Source of nonlinearity in echo-time-dependent BOLD fMRI. Magnetic Resonance In Medicine 2006;55(6):1281–1290. [PubMed: 16700023]
37. Boxerman JL, Bandettini PA, Kwong KK, Baker JR, Davis TL, Rosen BR, Weisskoff RM. The Intravascular Contribution To Fmri Signal Change - Monte-Carlo Modeling And Diffusion-Weighted Studies In-Vivo. Magn Reson Med 1995;34(1):4–10. [PubMed: 7674897]
38. Song AW, Wong EC, Tan SG, Hyde JS. Diffusion weighted fMRI at 1.5 T. Magn Reson Med 1996;35(2):155–158. [PubMed: 8622577]
39. Jochimsen TH, Norris DG, Mildner T, Moller HE. Quantifying the intra- and extravascular contributions to spin-echo fMRI at 3 T. Magn Reson Med 2004;52(4):724–732. [PubMed: 15389950]
40. Kim SG, Harel N, Jin T, Kim T, Lee P, Zhao FQ. Cerebral blood volume MRI with intravascular superparamagnetic iron oxide nanoparticles. Nmr Biomed 2013;26(8):949–962. [PubMed: 23208650]
41. Jin T, Kim SG. Characterization of non-hemodynamic functional signal measured by spin-lock fMRI. Neuroimage 2013;78:385–395. [PubMed: 23618601]
42. Lu H, Scholl CA, Zuo Y, Stein EA, Yang YH. Quantifying the blood oxygenation level dependent effect in cerebral blood volume-weighted functional MRI at 9.4T. Magn Reson Med 2007;58(3):616–621. [PubMed: 17763339]
43. Su C, Liu C, Zhao L, Jiang J, Zhang J, Li S, Zhu W, Wang J. Amide Proton Transfer Imaging Allows Detection of Glioma Grades and Tumor Proliferation: Comparison with Ki-67 Expression and Proton MR Spectroscopy Imaging. Am J Neuroradiol 2017;38(9):1702–1709. [PubMed: 28729292]
44. Gochberg DF, Gore JC. Quantitative magnetization transfer imaging via selective inversion recovery with short repetition times. Magn Reson Med 2007;57(2):437–441. [PubMed: 17260381]
45. Stejskal EO, Tanner JE. Spin Diffusion Measurements: Spin Echoes In the Presence Of a Time-Dependent Field Gradient. J Chem Phys 1965;42(1):288-+.
46. Zaiss M, Schmitt B, Bachert P. Quantitative separation of CEST effect from magnetization transfer and spillover effects by Lorentzian-line-fit analysis of z-spectra. J Magn Reson 2011;211(2):149–155. [PubMed: 21641247]
47. Zaiss M, Zu ZL, Xu JZ, Schuenke P, Gochberg DF, Gore JC, Ladd ME, Bachert P. A combined analytical solution for chemical exchange saturation transfer and semi-solid magnetization transfer. Nmr Biomed 2015;28(2):217–230. [PubMed: 25504828]
48. Zu ZL, Li H, Xu JZ, Zaiss M, Li K, Does MD, Gore JC, Gochberg DF. Measurement of APT using a combined CERT-AREX approach with varying duty cycles. Magnetic Resonance Imaging 2017;17(42):22–31.
49. Zhang XY, Wang F, Li H, Xu JZ, Gochberg DF, Gore JC, Zu ZL. Accuracy in the quantification of chemical exchange saturation transfer (CEST) and relayed nuclear Overhauser enhancement (rNOE) saturation transfer effects. Nmr Biomed 2017;30(7).

50. Zhang XY, Wang F, Li H, Xu JZ, Gochberg DF, Gore JC, Zu ZL. CEST imaging of fast exchanging amine pools with corrections for competing effects at 9.4 T. Nmr Biomed 2017;30(7).

51. Sandor P, Put JC, Dejong W, Dewied D. Continuous Measurement Of Cerebral Blood-Volume In Rats with the Photoelectric Technique - Effect Of Morphine And Naloxone. Life Sci 1986;39(18):1657–1665. [PubMed: 3773640]

52. Chugh BP, Lerch JP, Yu LX, Pienkowski M, Harrison RV, Henkelman RM, Sled JG. Measurement of cerebral blood volume in mouse brain regions using micro-computed tomography. Neuroimage 2009;47(4):1312–1318. [PubMed: 19362597]

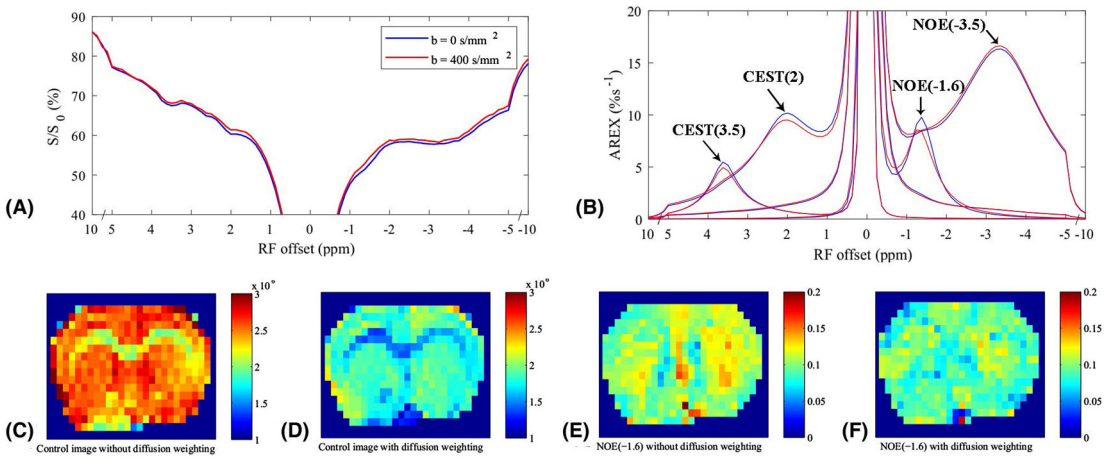

Figure 1.

Average CEST Z-spectra (a) and AREX spectra (b) for each pool from the whole brain of 5 rat brains with a diffusion-weighting of b = 0 s/mm^2 (blue) and 400 s/mm^2 (red), respectively. Control images without (c) and with (d) the diffusion weighting, respectively, from a representative rat brain. NOE(−1.6) images without (e) and with (f) the diffusion weighting, respectively, from a representative rat brain.

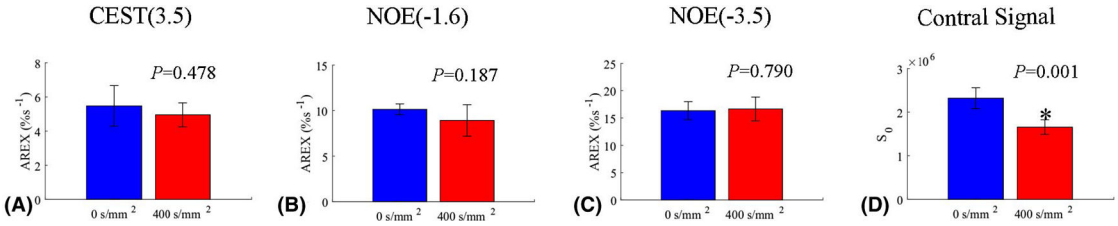

Figure 2.

Statistical analysis of AREX values for CEST(3.5) (a), NOE(−1.6) (b), and NOE(−3.5) (c) as well as control signals (d) from the whole brain acquired with a diffusion-weighting of b = 0 s/mm^2 (blue) and 400 s/mm^2 (red), respectively.

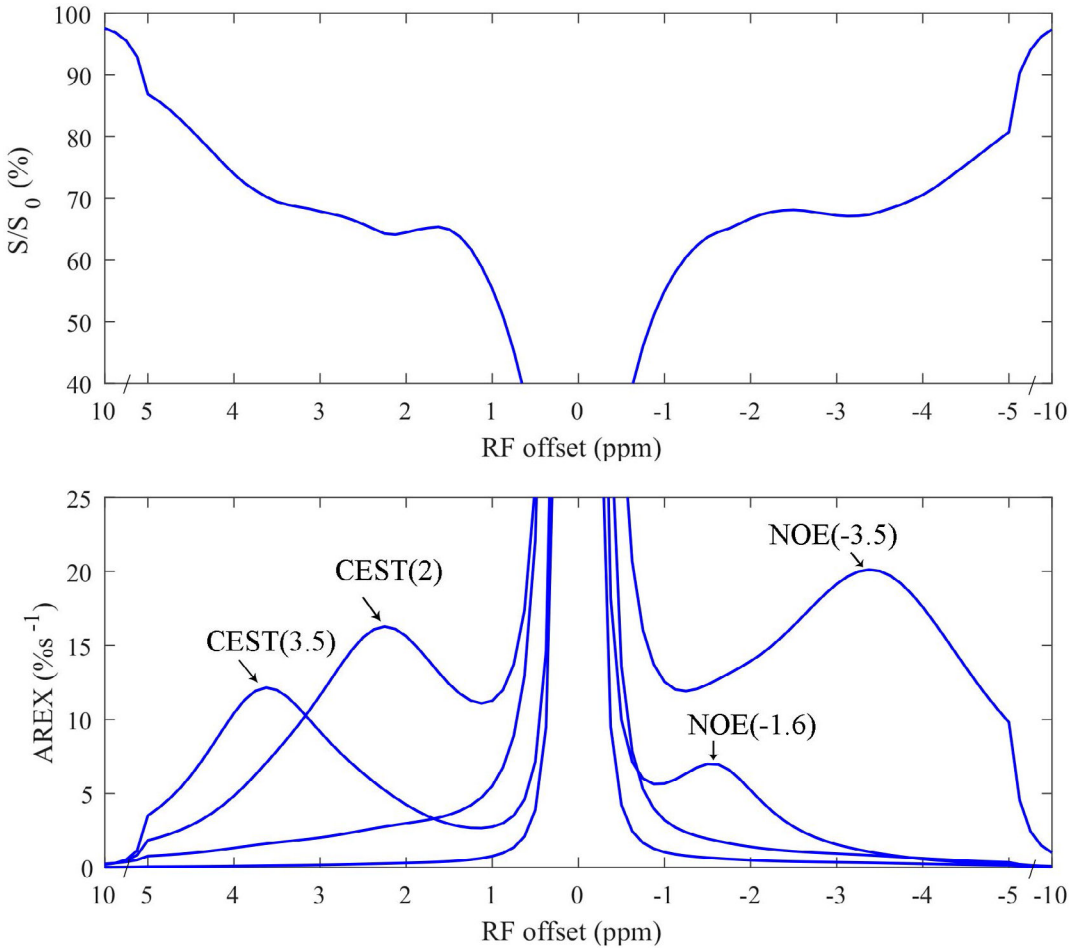

Figure 3.
CEST Z-spectra (upper) and AREX spectra for each pool (lower) from ex vivo arterial blood.

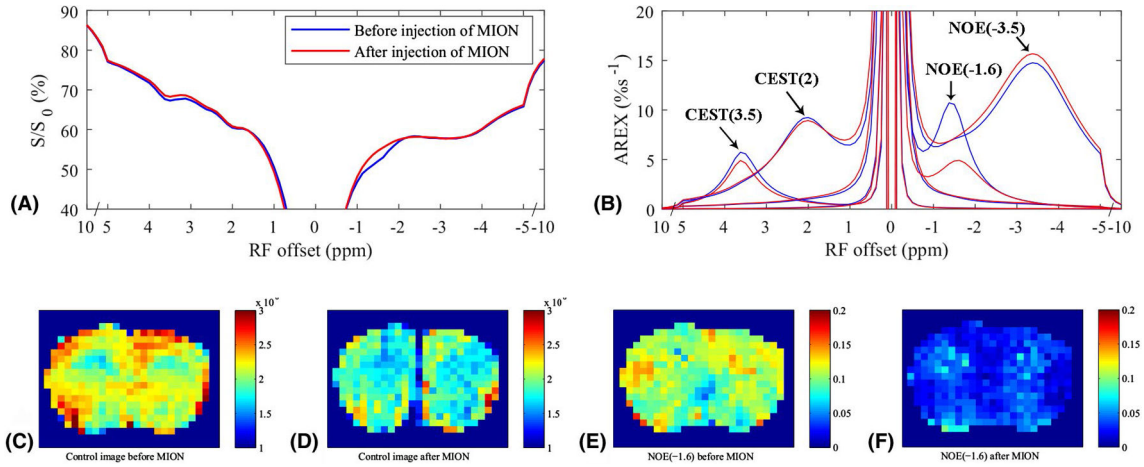

Figure 4.

Average CEST Z-spectra (a) and AREX spectra (b) for each pool from the whole brain of 5 rat brains before (blue) and after (red) the injection of 5mg/kg MION, respectively. Control images before (c) and after (d) the injection of MION, respectively, from a representative rat brain. NOE(−1.6) images before (e) and after (f) the injection of MION, respectively, from a representative rat brain.

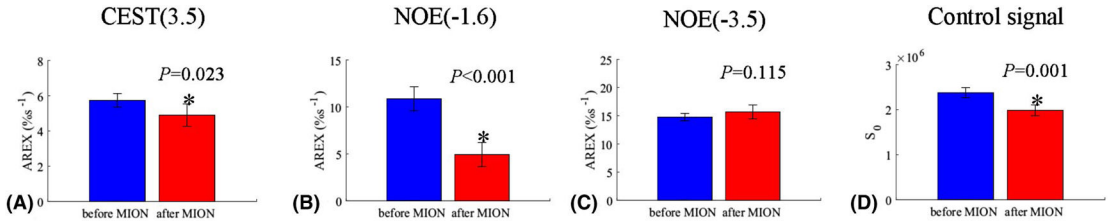

Figure 5.

Statistical analysis of AREX values for CEST(3.5) (a), NOE(−1.6) (b), and NOE(−3.5) (c) as well as control signals (d) from the whole brain acquired before (blue) and after (red) injection of 5mg/kg MION, respectively.